

HAFFNER 16: A YOUNG MOVING GROUP IN THE MAKING

T. J. Davidge

*Dominion Astrophysical Observatory,
National Research Council of Canada, 5071 West Saanich Road,
Victoria, BC Canada V9E 2E7*

Eleazar R. Carrasco, Claudia Winge, Peter Pessev, Benoit Neichel, Fabrice Vidal
Gemini Observatory/AURA, Southern Operations Center, Casilla 603, La Serena, Chile

Francois Rigaut

*Australian National University, Research School of Astronomy and Astrophysics,
Mount Stromlo Observatory, Cotter Road,
Weston, ACT 2611, Australia*

ABSTRACT

The photometric properties of main sequence (MS) and pre-main sequence (PMS) stars in the young cluster Haffner 16 are examined using images recorded with the Gemini South Adaptive Optics Imager (GSAOI) and corrected for atmospheric blurring by the Gemini Multi-Conjugate Adaptive Optics System (GeMS). A rich population of PMS stars is identified, and comparisons with isochrones suggest an age $\lesssim 10$ Myr assuming a distance modulus of 13.5 ($D = 5$ kpc). This age is consistent with that estimated from the lower cut-off of the MS on the K -band luminosity function, and is ~ 2 Myr younger than the age found from bright MS stars at visible wavelengths. When compared with the solar neighborhood, Haffner 16 is roughly a factor of two deficient in objects with sub-solar masses. PMS objects in the cluster are also more uniformly distributed on the sky than bright MS stars. It is suggested that Haffner 16 is dynamically evolved, and that it is shedding protostars with sub-solar masses. Young low

¹Based on observations obtained at the Gemini Observatory, which is operated by the Association of Universities for Research in Astronomy, Inc., under a cooperative agreement with the NSF on behalf of the Gemini partnership: the National Science Foundation (United States), the National Research Council (Canada), CONICYT (Chile), the Australian Research Council (Australia), Ministério da Ciência, Tecnologia e Inovação (Brazil) and Ministerio de Ciencia, Tecnología e Innovación Productiva (Argentina).

mass clusters like Haffner 16 are one possible source of PMS stars in the field. The cluster will probably evolve on time scales of $\sim 100 - 1000$ Myr into a diffuse moving group with a mass function that is very different from that which prevailed early in its life.

Subject headings: Star Clusters and Associations

1. INTRODUCTION

The total mass of a star cluster plays a key role in defining the pace of its evolution. While cluster mass affects the time scale of dynamical evolution in a direct manner, it may also influence cluster evolution in more subtle ways. Feedback from massive stars may disrupt a cluster if substantial mass outflow is induced while the cluster is in a gas-rich, pre-virialized state (e.g. Smith et al. 2011). However, such feedback-driven mass loss may not occur early-on in low mass clusters as there is a low probability that massive hot stars will form in systems with stellar masses less than a few hundred times solar assuming a solar neighborhood mass function (MF). Clusters that lack stars with evolutionary timescales that are shorter than a few cluster crossing times may then not be subject to the catastrophic mass loss that is thought to spur ‘infant mortality’ (Lada & Lada 2003), although environmental mechanisms might still contribute to their early demise (e.g. Kruijssen et al. 2012).

Cluster mass may also influence stellar content. While the characteristic masses of stars are primarily defined by physical constants rather than environmental properties (Krumholz 2011), the global characteristics of the host cluster may still influence the observed MF. If a large-scale loss of gas does not occur early-on then a cluster may retain low mass stars that would otherwise be lost (Pelpussey & Portegies Zwart 2012) for a longer period of time. Radiation and winds from hot stars can also erode proto-stellar accretion disks, thereby choking growth and limiting the minimum mass of MS stars (e.g. De Marchi et al. 2011b). If very massive stars do not form then circumstellar accretion disks may survive for longer periods of time than in more massive clusters. The minimum stellar mass in low mass clusters may then differ from that in more massive systems.

Low mass clusters are expected to form in large numbers, and so are significant contributors to the field star population. Studies of low mass clusters in the early stages of their evolution may then provide insights into the overall properties of field stars, such as the observed MF and the binary frequency (e.g. Marks & Kroupa 2011). Haffner 16 is an open cluster with a mass of a few hundred solar masses that is located at Galactic co-ordinates $\ell = 0^\circ 5$ and $b = 242^\circ 1$ (i.e. outside of the Solar circle). Vogt & Moffat (1972) present a

color-magnitude diagram (CMD) that shows bright main sequence (MS) stars indicative of a young age. McSwain & Gies (2005) measure an age of $\log(t_{yr}) = 7.08$ from multicolor CCD photometry, and assign a distance of 3.2 kpc, placing Haffner 16 in the Perseus Arm. They also find 19 B stars that may be cluster members, one of which is a possible Be star.

Narrow-band $H\alpha$ measurements discussed by McSwain & Gies (2005) indicate that there are a number of emission line sources with a range of broad-band colors in and around Haffner 16. Given the young age of the cluster, this suggests that there may be a substantial population of actively accreting pre-main sequence (PMS) stars. In the present paper, broad and narrow-band near-infrared images recorded with the Gemini South Adaptive Optics Imager (GSAOI) and corrected for atmospheric blurring by the Gemini Multi-conjugate Adaptive Optics (AO) System (GeMS) are used to examine the photometric properties and spatial distribution of stars and proto-stars in Haffner 16. The use of GeMS is of interest for such an investigation given the compact nature of Haffner 16, and the potential for crowding if low mass stars are present in moderately large numbers.

2. OBSERVATIONS

The images were recorded with GSAOI+GEMS (McGregor et al. 2004; Carrasco et al. 2012, Rigaut et al. 2012; Neichel et al. 2012) as part of program GS-2012B-SV-409. GSAOI is an imager that is designed to be used with GEMS. The GSAOI detector is a mosaic of four 2048×2048 Rockwell Hawaii-2RG arrays, deployed in a 2×2 format. A 85×85 arcsec² field is imaged with 0.02 arcsec per pixel sampling. There are ~ 3 arcsec gaps between the arrays. Haffner 16 fits within a single GSAOI pointing.

GeMS produces image profiles that are more spatially uniform than would be delivered by a classical single beacon AO system over a similarly-sized field (e.g. Davidge 2010). This is done using information provided by five laser guide stars (LGSs), three natural guide stars (NGSs), and an on-detector guider to monitor wavefront distortions. The three NGSs used for the Haffner 16 observations were selected based on their brightness and location. The NGSs more-or-less define the apexes of an equalatorial triangle-shaped asterism that spans most of the GSAOI science field. While the stability of the image profile and the level of correction delivered by GeMS depends on a number of factors, including guide star brightness, wind speed in the dominant turbulent layers etc, an asterism with this shape typically provides a reasonably stable point spread function (PSF) across most of the GSAOI field.

Images were recorded through J , Ks , and $Br\gamma$ filters ¹. Two different exposure times were used to broaden the magnitude range that was sampled. Three 5 sec exposures were recorded per filter to cover moderately bright cluster members, while 5×30 sec exposures in J and Ks and 5×60 sec exposures in $Br\gamma$ were recorded to sample fainter stars. An on-sky dither pattern with a throw of a few arcsec along the east-west axis was employed to allow coverage in one of the gaps in the detector mosaic.

The initial processing of the data followed standard procedures for near-infrared images. Steps included dark subtraction, flat-fielding, and the subtraction of calibration frames that monitor thermal emission from warm objects along the optical path, such as dust on the GSAOI entrance window. The calibration images required for the last step were constructed by computing – on a filter-by-filter basis – the median signal at each pixel on the detector mosaic from all of the long exposure images recorded for the program. A mean sky level was subtracted from each image to correct for variations in sky brightness before computing the median. Since a number of clusters were observed for this program, and the data were recorded with a dither pattern, then the median signal at each pixel is more-or-less free of contributions from bright objects on the sky, and so monitors the thermal emission signatures that remain after the flat-field pattern is removed.

The processed images in each filter were aligned to correct for the dither offsets. The final step before stacking the aligned images was to correct for distortions introduced by the system optics. These are most severe near the edge of the science field, and affect the data in two ways. First, the angular scale over which the distortion changes is a few tenths of an arcsec, and image combination is complicated if – as with these observations – dither offsets exceed these scales. Second, the distortions are chromatic, and so sources near the edge of the science field have different filter-to-filter locations if the individual images are aligned near the center of the science field. If left uncorrected, these distortions complicate the matching of photometric measurements recorded in different filters as well as the investigation of the spatial distribution of objects. The distortions were corrected in a differential way by mapping the J and $Br\gamma$ images into the reference frame defined by the Ks filter using the GEOMAP and GEOTRAN tasks in IRAF.

3. PHOTOMETRIC MEASUREMENTS

Stellar brightnesses were measured with the PSF-fitting routine ALLSTAR (Stetson & Harris 1988). The source catalogues, PSFs, and preliminary magnitudes that serve as input

¹Various properties of these filters are described at <http://www.gemini.edu/sciops/instruments/gsaoi/instrument-descripti>

to ALLSTAR were obtained from tasks in the DAOPHOT (Stetson 1987) package. The PSF in each filter was constructed from 14 isolated, high S/N ratio stars located throughout the field. The photometric calibration was based on standard star observations that were made on the same night as the Haffner 16 observations, and the instrumental magnitudes in Ks were transformed into K magnitudes ².

The uniformity of the image profiles is investigated in Figure 1, which shows the FWHMs of the PSF stars; the final deep Ks image is also shown. The FWHMs in the final $Br\gamma$ images are similar to those in Ks . Even though the data were recorded during relatively poor seeing conditions (85%ile image quality; ~ 0.8 arcsec FWHM in Ks), the corrected images have $\text{FWHM} \leq 0.16$ arcsec in Ks , demonstrating that GeMS can deliver substantial improvements in image quality over the GSAOI field even during less-than-optimal conditions. The level of correction and spatial uniformity of the image profile degrades towards shorter wavelengths, as the size of the isoplanatic patch shrinks. This results in a larger mean FWHM and more variation in the FWHM in J than in Ks . The uniformity of the PSF and the mean FWHM during typical seeing conditions will be much better than shown in Figure 1.

The photometry was performed using spatially-variable PSFs to account for variations in FWHM. Because GeMS did a reasonable job of correcting the PSF across the GSAOI field, only a low-order fitting function was employed. A much more complicated PSF model would be required for AO images corrected with only a single beacon, even over angular scales that are only a fraction of the GSAOI field.

Artificial star experiments were run to investigate sample completeness and uncertainties in the photometry. Artificial stars were generated using the empirical PSFs that were constructed from the final images, and were assigned colors that follow the main plume of points in the CMD. As with on-sky objects, artificial stars were only considered to be detected if they were recovered in both J and Ks . The recovery statistics of artificial stars indicate that incompleteness becomes an issue when $K \gtrsim 18 - 18.5$. This matches the approximate magnitude in the CMD where the density of objects noticeably starts to drop towards fainter magnitudes (Section 4.1).

²Throughout this paper Ks is used to refer to the filter, while K refers to the transformed magnitudes.

4. CMDs AND LUMINOSITY FUNCTIONS

4.1. The $(K, J - K)$ CMD

The $(K, J - K)$ CMD of Haffner 16 is shown in the left hand panel of Figure 2. The green error bars indicate the $\pm 2\sigma$ dispersion in $J - K$ at $K = 17$ and 18 calculated from the artificial experiments, and it is encouraging that the predicted dispersion matches the observed width of the red plume centered near $J - K = 0.9$ at $K = 18$. The artificial star experiments indicate that the positional scatter between objects with $K \lesssim 17$ on the CMD is due to differences in their intrinsic properties, rather than uncertainties in the photometry.

There is the potential for substantial field star contamination given that Haffner 16 is at a low Galactic latitude. However, as the cluster just fits within the GSAOI science field, then the density of field stars can not be measured from these data alone. Insights into field star contamination were gleaned by examining the 2MASS $(K, J - K)$ CMD of an area near Haffner 16. While the 2MASS observations are substantially shallower than the GeMS images, the magnitude range sampled by 2MASS still overlaps with the region containing the brightest PMS objects in Haffner 16 (see below).

The brightnesses of objects in J and K image sections retrieved from the 2MASS archive were measured with ALLSTAR. The resulting $(K, J - K)$ CMD of objects that are immediately to the south of Haffner 16, with the photometric calibration set using zeropoint information in the 2MASS image headers, is shown in the left hand panel of Figure 3. The 2MASS field star CMD can be compared with the GeMS CMD of Haffner 16, which is shown in the right hand panel of the figure. A comparison of the two panels indicates that field stars are present in the color and magnitude ranges populated by objects in Haffner 16. However, the projected number density of field stars is much lower than that of cluster members. To demonstrate this, the number of field stars expected in various regions of the CMD in the GSAOI field are indicated in brackets in the right hand panel of the figure. The expected number of field stars along the cluster sequence is substantially lower than the number of objects in the GeMS CMD, indicating that the majority of objects in the Haffner 16 CMD that have $K < 15$ are not field stars.

The 2MASS data provide a useful check of the GeMS photometric calibration. The 2MASS CMD of objects in the same field that is sampled with GeMS is shown in the right hand panel of Figure 3. There are substantial differences between the angular resolution and photometric depth of the 2MASS and GeMS datasets, and some of the stars in Haffner 16 are almost certainly photometric variables. Still, the GeMS and 2MASS CMDs are very similar.

The 2MASS images also can be used to gain insights into the total brightness and mass of Haffner 16. The distribution of stars in the 2MASS image indicates that Haffner 16 has a radius ~ 1 arcmin and a total brightness $M_K = -3.2$ if the distance modulus, μ_0 , is 12.50 and $M_K = -4.2$ if $\mu_0 = 13.50$. The Bressan et al. (2012) models predict that a $1M_\odot$ SSP with an age near 10 Myr will have $M_K = 2.8$, and so the estimated total mass of Haffner 16 is $\sim 260 M_\odot$ if $\mu_0 = 12.50$, and $630 M_\odot$ if $\mu_0 = 13.50$.

The middle and right hand panels of Figure 2 show comparisons between the $(K, J-K)$ CMD of Haffner 16 and $Z = 0.016$ sequences from the Padova Isochrones (Bressan et al. 2012), which were downloaded from the Padova Observatory web site³. These models include PMS evolution, making them useful for examining the stellar contents of young clusters like Haffner 16. The approximate magnitude of the main sequence cut-off (MSCO), which is the faint end of the MS defined by stars that are relaxing onto the MS, is marked for each model. We caution that there are numerous uncertainties in the input physics of the PMS phase of evolution (e.g. Seiss 2001). For example, the mechanics of accretion affects profoundly the luminosities of PMS models (e.g. Offner & McKee 2011).

The distance and color excess measured by McSwain & Gies (2005) have been used to place the isochrones in the middle panel of Figure 2. That the isochrones in this panel agree with the near-vertical red plume of stars with $K > 16.5$ suggests that the reddening is reasonable. However, many of the sources in the upper half of the CMD, the vast majority of which are probably cluster members (e.g. the comparisons in Figure 3), fall blueward of the isochrones if $\mu_0 = 12.50$. The PMS stars have ages between 10 and 25 Myr with this distance modulus, and many probable PMS objects with K between 15 and 15.5 fall blueward of the 25 Myr isochrone.

The poor agreement with the blue envelope on the CMD can be eased – while still maintaining a good match with the lower portion of the CMD – if a larger distance modulus is adopted. This is demonstrated in the right hand panel of Figure 2, where comparisons are made with isochrones assuming $\mu_0 = 13.5$. The group of points with $J - K \sim 0$ and K between 15 and 15.5 that fall blueward of the 25 Myr isochrone in the middle panel now fall near the 10 Myr isochrone, and thus have a predicted age that is in better agreement with that of other PMS stars in Haffner 16. A distance modulus of 13.5 is also favored given the presence of numerous red emission line sources (McSwain & Gies 2005), which are probably PMS stars and would not be expected to show line emission if they were much older than ~ 10 Myr (e.g. de Marchi et al. 2011). Using the 10 Myr isochrone in the right hand panel of Figure 3 as a guide, the location of points on the CMD suggest that the MSCO occurs

³<http://stev.oapd.inaf.it/cgi-bin/cmd>

near $K \sim 15.4$. The issue of distance aside, it is clear from Figure 2 that Haffner 16 harbors a rich population of PMS stars, as expected given its young age.

4.2. Br γ emission

The comparisons with the isochrones suggest that the majority of bright objects in Haffner 16 are MS stars, and that PMS objects dominate at fainter magnitudes. If the PMS stars in Haffner 16 are still accreting gas, which might be expected if they have near-solar metallicities and ages ≤ 10 Myr (e.g. De Marchi et al. 2011), then they may show neutral Hydrogen in emission. Not all PMS stars will show such emission, as the accretion rate varies with time (Haisch et al. 2001; Calvet et al. 2000; Fedele et al. 2010). The rate of accretion, and hence emission line strength, also depends on (1) metallicity, in the sense that at a given age the accretion rate increases as metallicity is lowered (e.g. de Marchi et al. 2011), as well as (2) age, with the rate of accretion among Galactic PMS objects dropping by 1.6 dex per decade in age (e.g. Figure 9 of de Marchi et al. 2011).

Br γ falls within the wavelength range covered by GeMS, and Br γ emission has been detected from protostars (e.g. Connelley & Green 2009; Beck et al. 2010; Doneshaw & Brittain 2011). Because it involves a higher excitation transition, Br γ will not be as strong as H α , and previous studies have measured equivalent widths for Br $\gamma \leq 10$ Å. The effective width of the Br γ filter is 320Å, and so the detection of emission with an equivalent width of a few Å requires photometry with a reliability of a few hundredths of a magnitude.

The $(K, Br\gamma - K)$ diagram of Haffner 16 is shown in the upper panel of Figure 4. The GSAOI K_s and Br γ filters have similar mean throughputs, and so the Br γ measurements were calibrated by scaling the K -band zeropoint according to the effective wavelength ranges of the two filters so that $m_{Br\gamma} \approx m_{K_s}$. There is considerable scatter in the $Br\gamma - K$ values; still, between $K = 13$ and 17 there is a tendency for $Br\gamma - K$ to decrease towards fainter K . Near $K = 17.25$ the $Br\gamma - K$ distribution changes, as objects with $Br\gamma - K \gtrsim 0.1$ appear in large numbers. A Kolmogorov-Smirnov test indicates that the $Br\gamma - K$ distributions in the intervals $K = 14.75$ to 17.25 and $K = 17.25$ to 18.25 differ at more than the 99% confidence level.

The 1σ dispersion in $Br\gamma - K$ at $K = 17$ calculated from the artificial star experiments is ± 0.04 magnitudes, and this matches the width of the $Br\gamma - K$ distribution at various K magnitudes in the top panel of Figure 4. While photometric uncertainties of this size make it difficult to detect individual sources of Br γ emission with equivalent widths of a few Å, random uncertainties can be suppressed by examining mean Br $\gamma - K$ values. The mean

values of $Br\gamma - K$ in ± 0.5 magnitude intervals in K are shown in the lower panel of Figure 4. An iterative $\pm 2.5\sigma$ rejection filter was applied to suppress outliers, and the errorbars show the formal $\pm 1\sigma$ uncertainties in the mean. $\langle Br\gamma - K \rangle$ is not constant over the range of K magnitudes investigated here, with $\langle Br\gamma - K \rangle$ at $K = 16.5$ differing from the means at $K = 15.5$ and 17.5 at almost the 3σ level. To further investigate the behaviour of $Br\gamma - K$ with magnitude, a Kolmogorov-Smirnov test was used to compare the $Br\gamma - K$ distributions of sources with K between 13 and 15 with those of sources having K between 15 and 17. The two $Br\gamma - K$ distributions differ at roughly the 99% confidence level, confirming that $\langle Br\gamma - K \rangle$ changes with magnitude.

The magnitude range in a system with an age of 10 Myr that the Padova isochrones predict will contain PMS sources is shown in the lower panel of Figure 4 for $\mu_0 = 12.5$ and 13.5 . $\langle Br\gamma - K \rangle$ is lowest in these magnitude ranges. While this is consistent with a large population of actively accreting PMS stars being present, we caution that the drop in $\langle Br\gamma - K \rangle$ is not conclusive proof of line emission – the lower values of $\langle Br\gamma - K \rangle$ near $K = 15.5$ and 16.5 could also reflect a change in $Br\gamma$ absorption strength, as expected if MS stars with cooler temperatures grow in number towards fainter K magnitudes. If the low $\langle Br\gamma - K \rangle$ values near $K = 16$ and 17 are due to PMS objects then a spectroscopic survey of this cluster should reveal a large number of $Br\gamma$ emission sources, and this could be checked by obtaining K -band spectra using a multi-object spectrograph such as Flamings 2.

There is a prominent population of objects with $K \geq 17$ that have comparatively high $Br\gamma - K$ values. We suspect that these are not cluster members, and so are not part of the PMS population and do not mark a change in cluster content that might be associated with – say – the MSCO. Rather, these are probably field stars. The comparatively large $Br\gamma - K$ values of these objects suggest that they might have relatively deep $Br\gamma$ absorption, such as occurs in MS stars with mid-A spectral-type. MS stars with this spectral type and apparent magnitude would be located at a distance of 8 kpc, placing them in the outer disc of the Galaxy. In fact, there are objects with $J - K$ between 0.3 and 0.7 and K between 17 and 18 in the $(K, J - K)$ CMD that form what appears to be a reddened A star sequence. However, the $Br\gamma - K$ colors of this particular set of objects tend to be *smaller* than those of objects with redder $J - K$ colors. Alternatively, the objects with large $Br\gamma - K$ colors and $K \geq 17$ might be very cool intrinsically faint foreground dwarf stars that have deep molecular absorption features in the wavelength range covered by the $Br\gamma$ filter (e.g. Geballe et al. 2002).

4.3. The Cluster Luminosity Function

The luminosity function (LF) of a cluster contains encoded information about its star-forming history (SFH) and the MF of its component stars. The ages of young clusters can be estimated from a change in source counts in the LF that occurs near the MSCO (e.g. Cignoni et al. 2010). The amplitude of this feature depends on a number of factors, including age, age dispersion, and the binning used to construct the LF. As demonstrated below, the Padova isochrones predict that in a simple stellar system with an age ≤ 10 Myr this feature will appear as a discontinuity with an amplitude ≥ 0.2 dex in a K LF with 0.5 magnitude binning. Ages estimated from this feature are of interest since they do not rely on stars near the main sequence turn-off, the numbers of which in low mass clusters may be prone to stochastic effects.

The K LF of Haffner 16 is shown in Figure 5. The LF has been corrected for field star contamination using star counts from the Robin et al. (2003) model Galaxy, which were obtained through the web interface ⁴. A uniform absorption distribution of 0.15 mag/kpc was assumed, and experiments indicate that the model counts do not vary substantially if the amount of extinction is doubled. The full range of stellar types and ages allowed by the model were included. The star count models agree to within a few percent with number counts between $K = 13.5$ and 15.0 obtained from 2MASS observations that sample the field near Haffner 16.

The LF tends to rise towards decreasing magnitudes, although there is a prominent notch near $K \sim 16$. Model LFs constructed from the Bressan et al. (2012) isochrones are shown in Figure 5, and these provide guidance for interpreting the observations. The models assume a Chabrier (2001) lognormal IMF and $Z=0.016$, and sequences with ages 6.5 and 10 Myr are shown. The models have been normalized to match the Haffner 16 number counts between $K = 16.25$ and 18.75, and results are shown for $\mu_0 = 12.5$ and 13.5.

Given the magnitude interval used for normalization, both models more-or-less fit the faint end of the LF. However, there are subtle differences within the magnitude interval used for normalization. With $\mu_0 = 12.5$ the models predict a trend that is systematically shallower than that observed, while for $\mu_0 = 13.5$ the models are systematically steeper.

Both the 6.5 and 10 Myr models tend to fall below the observations with $K \leq 15.5$ if $\mu_0 = 12.5$, and better agreement would not be achieved by considering models with older ages. Neither the 6.5 Myr nor the 10 Myr model predicts a drop in number counts near $K = 16$ if $\mu_0 = 12.5$. The 10 Myr model could be made to better match the number counts

⁴<http://model.obs-besancon.fr/>

with $K \leq 15.5$ if a 0.35 dex shift upwards were applied, although this would then produce a discrepancy between the models and observations when $K \geq 16.5$, in the sense that Haffner 16 would be deficient in lower mass PMS objects when compared with model predictions.

There is slightly better agreement with the observations if $\mu_0 = 13.5$. In this case the 10 Myr model matches the location – if not the amplitude – of the drop in number counts near $K = 16$. However, as with $\mu_0 = 12.5$, there is a discrepancy with the number counts at the bright end, in the sense that the agreement with the observed LF in the interval $K \leq 15.5$ could be improved by moving the models up by ~ 0.25 dex. There would then be a discrepancy between the models and observations at the faint end, in the sense that Haffner 16 would be deficient in low mass PMS objects when compared with model predictions.

The ratio of the numbers of stars with $K \leq 15.5$ and $K \geq 16.5$ is smaller than predicted by the model LFs for both distance moduli. This is not due to incompleteness, which only becomes significant for $K \geq 18.5$. Rather, to the extent that the models faithfully reproduce PMS evolution, then the comparisons in Figure 5 suggest that the MF in Haffner 16 is shallower than the Chabrier (2001) solar neighborhood relation. Later in the paper we will argue that this is likely a result of dynamical evolution.

5. THE SPATIAL DISTRIBUTION OF MS AND PMS OBJECTS

The spatial distribution of objects forms part of a cluster’s fossil record. The angular distributions of two groups of objects in Haffner 16 are investigated in this section: (1) bright main sequence (BMS) stars, which are defined to have K between 13 and 15, and (2) PMS sources, which have K between 15 and 17. For the purposes of defining these samples it has been assumed that $K = 15$ is the boundary between MS and PMS objects, based on the peak magnitude of the 10 Myr PMS sequence if $\mu_0 = 13.5$. The results presented below would not change markedly if the BMS/PMS dividing point was set at – say – $K = 15.5$.

The on-sky locations of the sources in the BMS and PMS samples are compared in Figure 6. There are differences in the distributions of the BMS and PMS samples. While the PMS sources are more-or-less uniformly distributed, BMS objects tend to avoid the peripheral areas of the GSAOI field, suggesting that they are more centrally concentrated.

The two-point correlation function (TPCF) is one means of examining the clustering properties of sources. The TPCF is generated by computing the separations between all possible pairings in a sample, and then dividing the resulting separation function (SF) by that of a set of randomly distributed sources located in the same detector geometry (e.g. including gaps between arrays) as the source data. The TPCFs of the BMS and PMS

samples, normalized using the SF of 10^4 randomly distributed sources and scaled according to the number of pairings in the real and artificial datasets, are compared in the top panel of Figure 7.

There is considerable bin-to-bin chatter in the TPCFs due to the small numbers of objects in the BMS and PMS samples. Still, the TPCFs of the BMS and PMS samples differ in a systematic way, in the sense that the TPCF of PMS objects is flatter than the TPCF of BMS objects. The PMS TPCF falls above that of BMS stars at separations > 65 arcsec, and below that of BMS stars for separations < 30 arcsec. There is also a modest peak in the TPCF of BMS objects in the bin that samples the smallest separations. This bin samples the angular scale where binaries, which have separations ≤ 0.04 parsec (Larson 1995), might be expected at the distance of Haffner 16. However, results presented later in this section suggest that this feature is not statistically significant.

The BMS and PMS samples have different levels of field star contamination. The Robin et al. (2003) model Galaxy predicts ~ 7 field stars in the BMS sample (out of 27 objects total), and 29 in the PMS sample (out of 58 objects total). The field star fraction in the PMS sample is thus $\sim 50\%$. To assess biases in the TPCF that might arise from field stars, simulations were run in which a population of objects with locations drawn from a uniform on-sky field star distribution were added to the BMS sample. The number of objects added to the BMS sample was selected so that the fraction of field stars was the same as in the PMS sample. The SF and TPCF of this BMS+Field star sample was then computed. This was repeated using different samples of randomly distributed stars, and the mean TPCF of the entire suite of realizations is compared with the PMS TPCF in the bottom panel of Figure 7. The error bars show the 1σ standard deviations about the mean signal at each separation.

The addition of objects with a uniform distribution on the sky introduces systematic trends in the BMS TPCF at separations > 65 arcsec, elevating the TPCF at these separations. Even so, the agreement with the signal in the PMS sample at large separations is poor. In addition, the TPCF of the mean BMS+Field sample consistently falls above that of the PMS TPCF at separations $5 - 20$ arcsec, indicating that the PMS objects show a lower degree of clustering on these angular scales than the BMS stars. We conclude that the objects in the PMS sample are more uniformly distributed than the BMS stars. Finally, there is considerable scatter in the BMS+Field star TPCF at the smallest separations, with no peak in the mean TPCF of BMS+Field objects due to close binaries. This indicates that the peak in the PMS sample in the smallest separation bin noted earlier is not a statistically robust feature.

6. SUMMARY & DISCUSSION

Near-infrared images obtained with GSAOI and GeMS on Gemini South have been used to investigate the stellar content of the young open cluster Haffner 16. Two distance moduli are considered: $\mu_0 = 12.50$ and $\mu_0 = 13.50$. The former is that measured by McSwain & Gies (2005) while the latter is found to produce better agreement with the $(K, J - K)$ CMD at the bright end and better internal consistency among the ages of PMS stars, which are present in large numbers in Haffner 16.

Isochrones predict that the PMS stars in Haffner 16 have ages $\lesssim 10$ Myr if $\mu_0 = 13.5$, and so some of these may show Hydrogen line emission. In fact, the $y - H\alpha$ colors of sources with $b - y > 0.1$ in Figure 12 of McSwain & Gies (2005) indicate that a rich population of $H\alpha$ emission sources are present in and around the cluster. McSwain & Gies (2005) argue that at least some of the emission line objects with blue colors may be Be stars, and we suspect that a substantial fraction of the faint, red $H\alpha$ sources in their data are PMS objects. The $\langle Br\gamma - K \rangle$ measurements discussed in Section 4.2 are also consistent with a significant fraction of the intermediate brightness PMS candidates in Haffner 16 having $Br\gamma$ in emission. Accretion activity might be expected to be long-lived in low mass clusters that did not form massive hot stars, as the disruption of accretion disks by feedback will be delayed. Velocity measurements would allow the membership status of the emission line objects to be assessed.

Comparisons with solar metallicity models suggest an age of ~ 10 Myr from the MSCO if $\mu_0 = 13.50$, and this is only a few Myr younger than the age estimated by McSwain & Gies (2005) from bright MS stars (albeit assuming a different distance modulus). A difference in ages measured from bright MS stars and the MSCO might be expected, especially for a low mass cluster like Haffner 16. Ages that are based on the properties of the brightest cluster stars are subject to stochastic effects, in the sense that the objects with the shortest lifetimes, such as very massive MS stars or stars in advanced stages of evolution, may be missing. The absence of such stars, whether due to stochastic effects or limitations imposed by the masses of star-forming clumps (e.g. Oey 2011), will skew ages estimated from the location of the MS turn-off to larger values. An age dispersion of a few Myr could also contribute to differences between age measurements made from MS and PMS stars in very young clusters. Star formation in at least some clusters has been found to occur over a 2 - 3 Myr time period (e.g. Hosokawa et al. 2011; Delgado et al. 2011; Bik et al. 2012, and references therein), while in giant star-forming complexes (e.g. De Marchi et al. 2011a) in-falling gas may fuel star-formation for even more extended periods of time (e.g. Garcia-Benito et al. 2011).

The data discussed here provide insights into the dynamical state of Haffner 16, and there are indications that it is dynamically evolved. To the extent that the Padova models faithfully track PMS evolution, the comparisons in Section 4 indicate that PMS stars fainter

than $K = 16.5$ occur in numbers that are lower than expected if stars in the cluster followed a Chabrier (2001) lognormal MF; Haffner 16 is deficient by roughly a factor of two in sub-solar mass PMS objects when compared with the solar neighborhood, and this holds for both distance moduli considered here. Also, evidence is presented in Section 5 that intermediate brightness PMS objects – which have sub-solar masses in Haffner 16 – are less clustered than the more massive MS stars. A trend of higher separations among PMS stars has been seen in other young clusters (e.g. Delgado et al. 2011), and is a signature of mass segregation.

The dynamical state of Haffner 16 can be assessed by comparing its age and dynamical timescale. The dynamical timescale is $\sim 1.1 - 1.7$ Myr using the radius and mass estimates computed from the 2MASS data in Section 4; thus, the cluster has a dynamical age of 6 - 9 crossing times. We have detected ~ 150 objects in Haffner 16, and an extrapolation of the LF to $K = 19 - 20$, which is the expected brightness of a $0.10 M_{\odot}$ proto-star with an age 10 Myr based on the Bressan et al. (2012) models, suggests that ~ 100 stars are below the faint limit if $\mu_0 = 12.50$, while 250 objects are missed if $\mu_0 = 13.5$. The ratio of relaxation to core-crossing time scales is then (Equation 4–9 of Binney & Tremaine 1987) ~ 6 ($\mu_0 = 12.5$) – 8 ($\mu_0 = 13.5$). The time scale for mass segregation is shorter than that for system relaxation, and so the detection of mass segregation signatures in Haffner 16 is then not surprising. A culling of low mass objects may also occur during early epochs if there is large scale gas removal (Pelupessy & Portegies Zwart 2012).

If it is assumed that the IMF of the Galactic thin disk is universal, then Haffner 16 has shed a significant fraction of its PMS stars. A diffuse collection of PMS stars might then be expected outside of the area probed with GeMS. Compact low mass clusters like Haffner 16 that have relatively short dynamical timescales may be a source of isolated groupings of PMS stars like those seen in the Galactic disk (e.g. Webb et al. 1999). Haffner 16 will almost certainly become progressively more diffuse on a timescale of ~ 100 Myr, eventually resembling a loosely concentrated moving group populated by a remnant ensemble of intermediate age stars with a MF that is very different from that with which it was born.

It is a pleasure to thank the anonymous referee for providing a timely and comprehensive report.

REFERENCES

- Beck, T. L., Bary, J. S., & McGregor, P.J. 2010, *ApJ*, 722, 1360
- Bik, A., Henning, Th., Stolte, A., et al. 2012, *ApJ*, 744, 87
- Binney, J., & Tremaine, S. 1987, *Galactic Dynamics* (Princeton:Princeton Univ. Press).
- Bressan, A., Marigo, P., Girardi, L., Salasnich, B., Dal Caro, C., Rubele, S., & Nanni, A., 2012, *MNRAS*, 427, 127
- Calvet, N., Hartmann, L., & Strom, E. 2000, in *Protostars and Planets*, ed. V. Mannings, A. Boss, & S. Russell (Tucson, Univ. Arizona Press), 377
- Carrasco, E. R., Edwards, M. L., McGregor, P. S. et al. 2012, *SPIE*, 8447, E0
- Chabrier, G. 2001, *ApJ*, 554, 1274
- Cignoni, M., Tosi, M., Sabbi, E., Nota, A., Degl’Innocenti, S., Prada Moroni, P. G., & Gallagher, J. S. 2010, *ApJ*, 712, L63
- Connelley, M. S., & Greene, T. P. 2009, *AJ*, 140, 1214
- Davidge, T. J. 2010, *ApJ*, 718, 1428
- De Marchi, G., Paresce, F., Panagia, N., et al. 2011a, *ApJ*, 739, 27
- De Marchi, G., Panagia, N., Romaniello, M., Saba, E., Sirianni, M., Prada Moroni, P. G., & Degl’innocenti, S. 2011b, *ApJ*, 740, 11
- Delgado, A. J., Alfaro, E. J., & Yun, J. L. 2011, *A&A*, 531, A141
- Doneshaw, B., & Brittain, S. 2011, *AJ*, 141, 46
- Fedele, D., van der Ancker, M., Henning, T., Jayawardhana, R., & Oliveira, J. 2010, *A&A*, 510, A72
- Garcia-Benito, R., Perez, E., Diaz, A. I., Apellaniz, J. M., & Cervino, M. 2011, *AJ*, 141, 126
- Geballe, T. R., Knapp, G. R., Leggett, S. K., et al. 2002, *ApJ*, 564, 466
- Haisch, K., Lada, E., & Lada, C. 2001, *ApJ*, 553, L153
- Hosokawa, T., Offner, S. S. R., & Krumholz, M. R. 2011, *ApJ*, 738, 140
- Krumholz, M. R. 2011, *ApJ*, 743, 11
- Kruijssen, J. M. D., Maschberger, T., Moeckel, N., Clarke, C. J., Bastian, N., & Bonnell, I. A. 2012, *MNRAS*, 419, 841
- Lada, C. J., & Lada, E. A. 2003, *ARA&A*, 41, 57
- Larson, R. B. 1995, *MNRAS*, 272, L213

- Marks, M., & Kroupa, P. 2011, MNRAS, 417, 1702
- McGregor, P., Hart, P., John, S. et al. 2004, SPIE, 5492, 1033
- McSwain, M. V., & Gies, D. R. 2005, ApJ, 622, 1052
- Neichel et al. 2012, SPIE, 8447, 84474
- Oey, M. S. 2011, ApJ, 739, L46
- Offner, S. S. R., & McKee, C. F. 2011, ApJ, 736, 53
- Pelupessy, F. I., & Portegies Zwart, S. 2012, MNRAS, 420, 1503
- Rigaut et al. 2012, SPIE, 8447, 84470
- Robin, A. C., Reyle, C., Derriere, S., & Picaud, S. 2003, A&A, 409, 523
- Siess, L. 2001, in From Darkness to Light, ASP Conf. Vol. 243, 581
- Smith, R., Fellhauer, M., Goodwin, S., & Assmann, P. 2011, MNRAS, 414, 3036
- Stetson, P. B. 1987, PASP, 99, 191
- Stetson, P. B., & Harris, W. E. 1988, AJ, 96, 909
- Vogt, N., & Moffat, A. F. J. 1972, A&AS, 7, 133
- Webb, R. A., Zuckerman, B., Platais, I., Patience, J., White, R. J., Schwartz, M. J., & McCarthy, C. 1999, ApJ, 512, L63

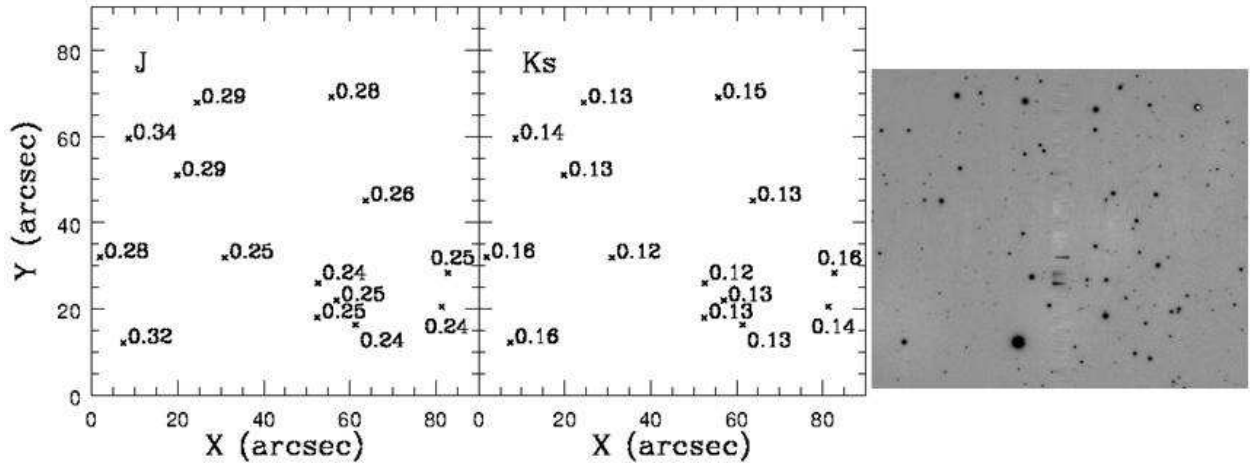


Fig. 1.— Full-width at half maximum (FWHM) measurements of the PSF stars. The FWHMs are in arcsec, while X and Y are angular offsets in the GSAOI field measured from one corner of the mosaic. The final deep Ks image is shown in the right hand panel. The mean FWHM in Ks is significantly smaller, and has much better spatial uniformity than in J .

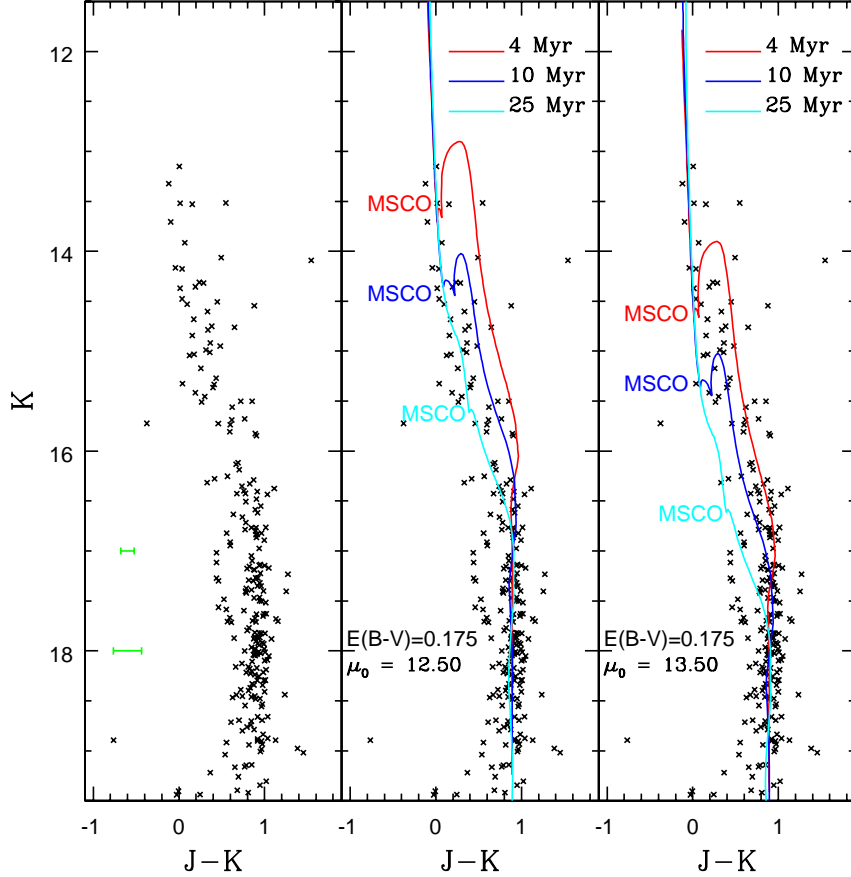


Fig. 2.— The $(K, J-K)$ CMD of Haffner 16 is shown in the left hand panel, where the green error bars indicate the $\pm 2\sigma$ dispersion in $J-K$ measured from artificial star experiments. The dispersion in $J-K$ at $K=18$ calculated from the artificial star experiments matches the width of the red plume near $J-K=0.9$. Comparisons with $Z=0.016$ sequences from the Padova Isochrones (Bressan et al. 2012) are made in the middle and right hand panels. The magnitude of the main sequence cut-off (MSCO), which is the faint limit of stars that have contracted onto the main sequence, is indicated for each isochrone. The models in the middle panel assume the reddening and distance modulus measured by McSwain & Gies (2005). While a number of objects fall blueward of the isochrones when $K \leq 17$, there is reasonable agreement with the vertical plume of objects with $J-K \sim 0.9$ near the faint end of the CMD, suggesting that the adopted reddening is reasonable. The result of adopting the same reddening but a larger distance modulus is examined in the right hand panel. A distance modulus of 13.5 produces better agreement with the blue envelope of the CMD, and the majority of PMS stars at intermediate brightnesses now fall between the 4 and 10 Myr isochrones. The distance modulus notwithstanding, it is evident that Haffner 16 contains a large population of PMS stars.

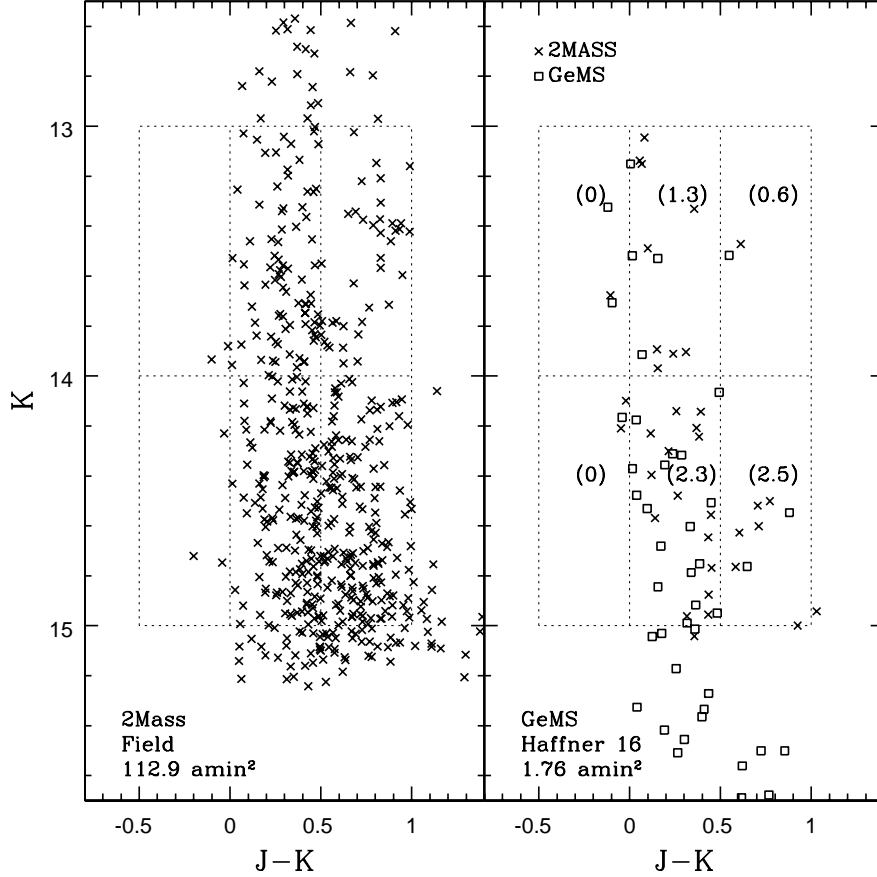


Fig. 3.— The 2MASS ($K, J - K$) CMD of a 112.9 arcmin^2 area that is immediately to the south of Haffner 16 is shown in the left hand panel, while the GeMS ($K, J - K$) CMD of Haffner 16 is plotted in the right hand panel. The numbers of field stars expected in various areas of the GeMS CMD, based on counts in the 2MASS CMD in the left hand panel, are indicated in brackets. These numbers indicate that the vast majority of objects with $K < 15$ in the GeMS CMD are not field stars. Also plotted in the right hand panel is the 2MASS CMD of Haffner 16, sampling the same area on the sky as GSAOI. The differences in angular resolution and photometric depth between the 2MASS and GeMS datasets notwithstanding, the two CMDs are very similar.

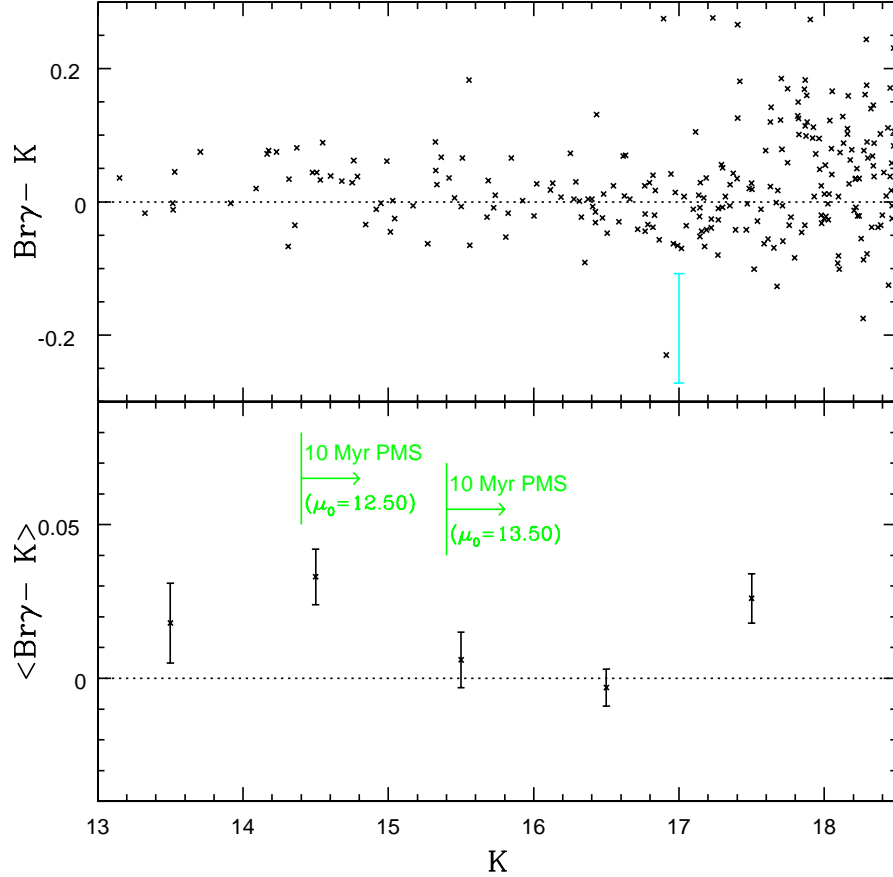


Fig. 4.— The $Br\gamma - K$ colors of individual sources is shown in the top panel, while the mean $Br\gamma - K$ colors in ± 0.5 magnitude K intervals are shown in the bottom panel. $Br\gamma$ emission will cause objects to have lower $Br\gamma - K$ colors than non-emitting sources. The cyan errorbar in the top panel is the $\pm 2\sigma$ dispersion in $Br\gamma - K$ at $K = 17$ calculated from the artificial star experiments, while the errorbars in the lower panel are the 1σ uncertainties in $\langle Br\gamma - K \rangle$. $Br\gamma - K = 0$ is indicated in each panel. The magnitude range where the Padova isochrones predict PMS stars should occur in a system with an age of 10 Myr is indicated in the lower panel for $\mu_0 = 12.50$ and 13.50 . $\langle Br\gamma - K \rangle$ is not constant, but changes with K , with $\langle Br\gamma - K \rangle$ being lowest in the magnitude range where PMS stars are expected. $\langle Br\gamma - K \rangle$ increases when $K \geq 17$, and a comparison with the top panel indicates that this is due at least in part to the onset of a population of objects with $Br\gamma - K \gtrsim 0.1$.

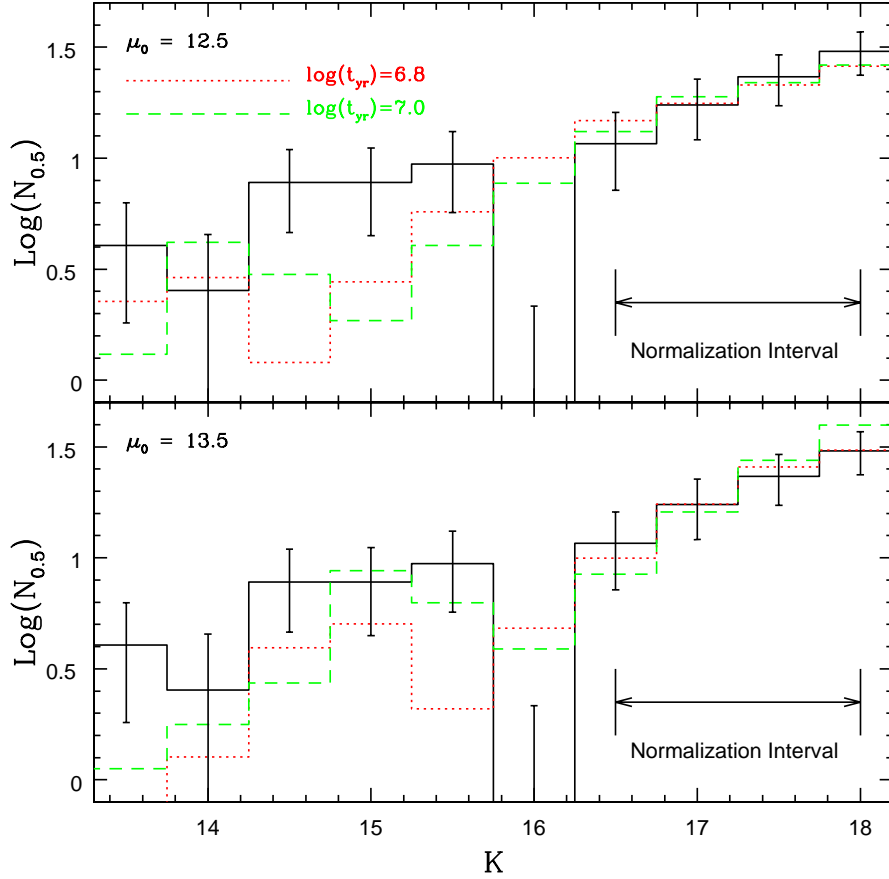


Fig. 5.— The K LF of Haffner 16. $N_{0.5}$ is the number of objects per 0.5 magnitude interval in K , corrected for field star contamination using results from the Robin et al. (2003) model Galaxy. The error bars are 1σ uncertainties based on counting statistics. Synthetic LFs constructed from $Z=0.016$ Bressan et al. (2012) models, with ages of $\log(t_{yr}) = 6.8$ (dotted line) and 7.0 (dashed line), are also shown. The models assume a Chabrier (2001) lognormal IMF, and have been scaled to match the observations in the magnitude interval indicated. Comparisons are shown for two distance moduli. The drop in the number counts near $K = 16$ can be reproduced – at least in location if not in amplitude – by the 10 Myr models with $\mu_0 = 13.5$. The models tend to fall below the observations when $K \leq 15.5$ for both distance moduli. This suggests that the MF of Haffner 16 is shallower than predicted by the models, and it is argued that this is likely a consequence of dynamical evolution.

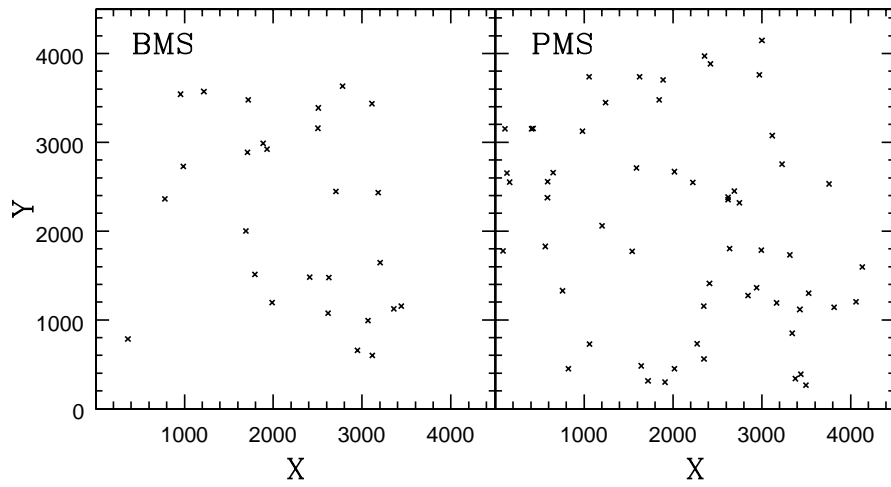


Fig. 6.— The spatial distribution of objects in the BMS and PMS samples. X and Y are GSAOI pixel locations in the co-ordinate system defined by the Ks observations (Section 2). Note that while the objects in the PMS sample are distributed more-or-less uniformly across the field, the BMS stars appear to be more centrally concentrated.

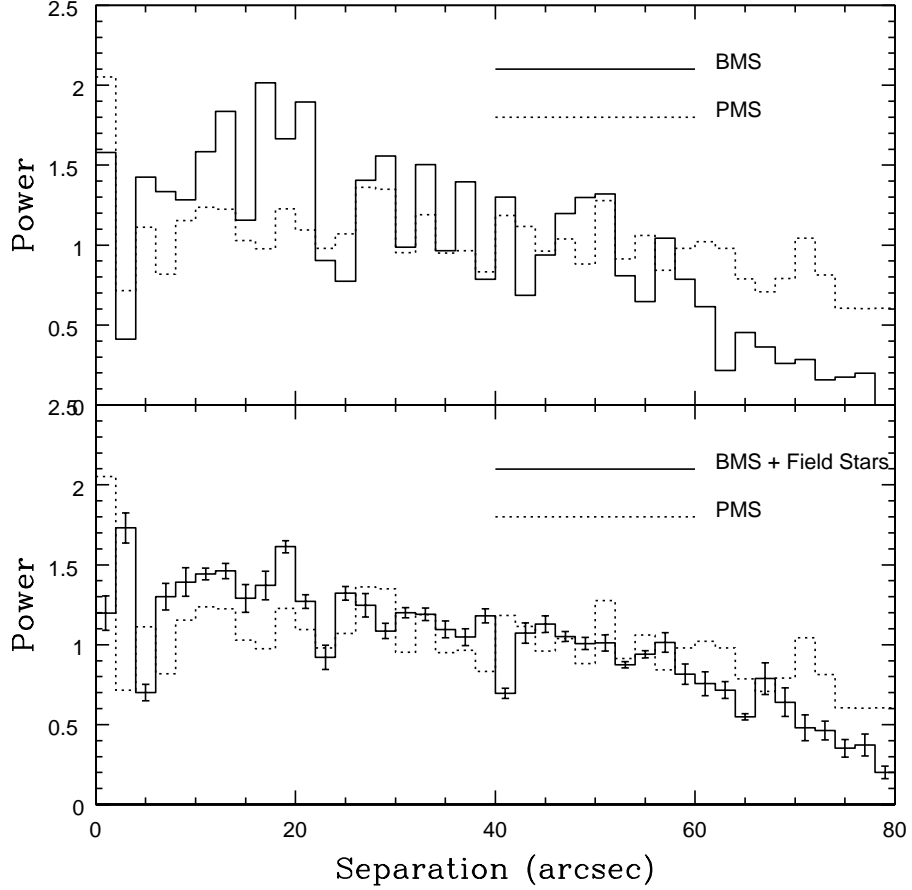


Fig. 7.— Top panel: The two-point correlations functions (TPCFs) of the BMS and PMS samples. The separation functions (SFs) of both samples have been divided by the SF of 10^4 randomly distributed sources, and then scaled according to the number of objects in the real and simulated samples. The TPCFs of the BMS and PMS sample differ, in that the PMS objects tend to have more power at separations > 60 arcsec, and less power at separations < 20 arcsec. Bottom panel: The solid line shows the average TPCF of a suite of simulations in which random objects, selected from a uniformly distributed population, were added to the BMS sample to simulate the 50% field star contamination in the PMS sample. The error bars show the 1σ standard deviation about the mean TPCF at each separation. Also shown is the TPCF of the PMS sample from the top panel. Differences remain between the TPCFs of the BMS and PMS samples after compensating for differences in field star fraction, in the sense that the TPCF of the PMS sample is flatter than that of the BMS+Field star sample. These experiments confirm that PMS stars in Haffner 16 are more loosely clustered than BMS stars.